A method to estimate the fractional fat volume within a ROI of a breast biopsy for WAXS applications: Animal tissue evaluation

Robert Y. Tang, Nancy McDonald, Curtis Laamanen, and Robert J. LeClair

Articles you may be interested in

WAXS fat subtraction model to estimate differential linear scattering coefficients of fatless breast tissue: Phantom materials evaluation
Med. Phys. **41**, 053501 (2014); 10.1118/1.4870982

Quantitative analysis of breast parenchymal patterns using 3D fibroglandular tissues segmented based on MRI
Med. Phys. **37**, 217 (2010); 10.1118/1.3271346

The tissue diagnostic instrument
Rev. Sci. Instrum. **80**, 054303 (2009); 10.1063/1.3127602
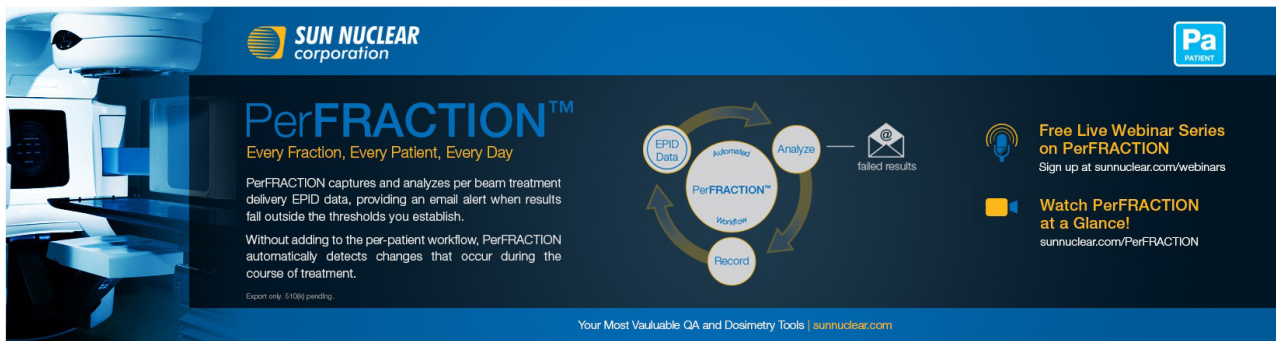
X-ray scattering for classifying tissue types associated with breast disease
Med. Phys. **35**, 4660 (2008); 10.1118/1.2977667

The development and testing of a digital PET phantom for the evaluation of tumor volume segmentation techniques
Med. Phys. **35**, 3331 (2008); 10.1118/1.2938518

A method to estimate the fractional fat volume within a ROI of a breast biopsy for WAXS applications: Animal tissue evaluation

Robert Y. Tang[a)]
Biomolecular Sciences Program, Laurentian University, 935 Ramsey Lake Road,
Sudbury, Ontario P3E 2C6, Canada

Nancy McDonald[b)] and Curtis Laamanen[c)]
Department of Physics, Laurentian University, 935 Ramsey Lake Road, Sudbury, Ontario P3E 2C6, Canada

Robert J. LeClair[d)]
Department of Physics, Laurentian University, 935 Ramsey Lake Road, Sudbury, Ontario P3E 2C6, Canada
and Biomolecular Sciences Program, Laurentian University, 935 Ramsey Lake Road, Sudbury,
Ontario P3E 2C6, Canada

Purpose: To develop a method to estimate the mean fractional volume of fat ($\overline{v}_{fat}$) within a region of interest (ROI) of a tissue sample for wide-angle x-ray scatter (WAXS) applications. A scatter signal from the ROI was obtained and use of $\overline{v}_{fat}$ in a WAXS fat subtraction model provided a way to estimate the differential linear scattering coefficient μ_s of the remaining fatless tissue.

Methods: The efficacy of the method was tested using animal tissue from a local butcher shop. Formalin fixed samples, 5 mm in diameter 4 mm thick, were prepared. The two main tissue types were fat and meat (fibrous). Pure as well as composite samples consisting of a mixture of the two tissue types were analyzed. For the latter samples, v_{fat} for the tissue columns of interest were extracted from corresponding pixels in CCD digital x-ray images using a calibration curve. The means $\overline{v}_{fat}$ were then calculated for use in a WAXS fat subtraction model. For the WAXS measurements, the samples were interrogated with a 2.7 mm diameter 50 kV beam and the 6° scattered photons were detected with a CdTe detector subtending a solid angle of 7.75×10^{-5} sr. Using the scatter spectrum, an estimate of the incident spectrum, and a scatter model, μ_s was determined for the tissue in the ROI. For the composite samples, a WAXS fat subtraction model was used to estimate the μ_s of the fibrous tissue in the ROI. This signal was compared to μ_s of fibrous tissue obtained using a pure fibrous sample.

Results: For chicken and beef composites, $\overline{v}_{fat} = 0.33 \pm 0.05$ and 0.32 ± 0.05, respectively. The subtractions of these fat components from the WAXS composite signals provided estimates of μ_s for chicken and beef fibrous tissue. The differences between the estimates and μ_s of fibrous obtained with a pure sample were calculated as a function of the momentum transfer x. A t-test showed that the mean of the differences did not vary from zero in a statistically significant way thereby validating the methods.

Conclusions: The methodology to estimate $\overline{v}_{fat}$ in a ROI of a tissue sample via CCD x-ray imaging was quantitatively accurate. The WAXS fat subtraction model allowed μ_s of fibrous tissue to be obtained from a ROI which had some fat. The fat estimation method coupled with the WAXS models can be used to compare μ_s coefficients of fibroglandular and cancerous breast tissue. © *2014 American Association of Physicists in Medicine.* [http://dx.doi.org/10.1118/1.4897384]

Key words: fat estimation, breast biopsies, CCD x-ray imaging, WAXS, CdTe, differential linear scattering coefficients, WAXS fat subtraction model

1. INTRODUCTION

The use of wide-angle x-ray scatter (WAXS) signals to diagnose cancer in breast biopsies is being investigated by various researchers.[1–15] The scatter signals are a function of the momentum transfer argument $x = \sin(\theta/2)/\lambda$ which combines their dependence on scatter angle θ and photon wavelength λ.

Farquharson *et al.*[1] recently reported results of combining x-ray fluorescence (XRF) and energy dispersive x-ray diffraction (EDXRD) for the classification of breast specimens. The former provided quantification of concentrations of K, Ca, Zn, Fe, Cu, Br, and Rb, whereas the latter provided their

coherent scattering properties. The data were incorporated into a multivariate model [i.e., principal component analysis and soft independent modeling of class analogies (SIMCA)].[8] Their findings were mapped to histological analysis of the samples. They suggest that their model can potentially be used to classify a small tissue sample as benign or malignant.

Elshemey *et al.*[3] measured the scatter signals at $\theta = 4°–70°$ ($\Delta\theta = 0.5°$) of 36 breast tissue samples using an x-ray diffractometer consisting of a Cu anode x-ray tube operating at 40 kV. The Cu Kα = 8.047 keV scattered photons were selected by a graphite monochromator and detected by a sodium iodide crystal. Scatter profiles were peak normalized and it was

concluded that characterization parameters (e.g., full width half maximum (FWHM), ratios of scatter intensities, and areas under the curve) could be useful for diagnostic evaluations. For example, FWHM mean values of 0.50 ± 0.16 nm^{-1} and 1.18 ± 0.28 nm^{-1} were found for, respectively, healthy and malignant tissue.

Changizi *et al.*[5] measured diffraction profiles of 131 breast biopsies using a HPGe detector positioned at $\theta = 6°$. A tungsten target x-ray tube operating at 55 kV was used. Differences in the peak positions were observed for normal, carcinoma, and benign tissue. The peak heights found for carcinoma were located at 1.55 ± 0.04 nm^{-1}, 1.73 ± 0.06 nm^{-1}, and 1.85 ± 0.05 nm^{-1}, while adipose/fibroglandular mixtures yielded peaks at 1.15 ± 0.06 nm^{-1} and 1.4 ± 0.05 nm^{-1}. The differences between fibrocystic changes (e.g., nonmalignant breast lumps) and carcinoma were insignificant and the different types of carcinomas could not be distinguished (e.g., ductal carcinoma and lobular carcinoma).

Oliveira *et al.*[6] investigated the use of a powder diffractometer consisting of an x-ray tube with a Cu anode, a graphite monochromator selecting K$\alpha = 8.047$ keV photons, and a sodium iodide detector. Scatter signals from $\theta = 5°–150°$ [$\Delta\theta = (1/3)°$] were measured for 40 samples initially identified with histology. The scatter profiles for water were measured and agreed with measurements by Morin.[16] Normal glandular tissue yielded a peak at 1.7 nm^{-1}. The diffraction patterns for glandular, benign, and malignant tissue showed similar shapes but differed in peak heights. A discriminant analysis was used to classify biopsies. A sensitivity of 95.6% and a specificity of 82.3% were found for differentiating normal fibroglandular and malignant tissue.

Ryan and Farquharson[8] used an energy dispersive x-ray system (W anode tube operating at 80 kV with a HPGe detector) to analyze 39 breast tissue samples. The samples were classified by histology as adipose, fibroadenoma, fibrocystic change, malignant, and normal fibrous tissue. The electron densities were estimated from Compton scatter measurements ($\theta = 30°$, 57.97 keV Kα2 radiation). The x-ray diffraction signatures were acquired at $\theta = 7.5°$ with a measurement time of 1 h for each sample. These data were used to classify the tissue via SIMCA methods with a sensitivity of 54% and specificity of 100%.

Clinical WAXS applications for diagnosing breast cancer in biopsies have not yet transpired. The three main breast tissue types are fat, fibroglandular (fibrous), and cancer. Fat has a scatter peak signal at $x = 1.1$ nm^{-1} because of triacylglycerol molecules.[17] To compare WAXS from a malignant cancer versus fibroglandular tissue is difficult, since fat is likely to be present in a biopsy. In this work, a method to estimate the mean fractional volume of fat $\overline{v}_{fat}$ within a region of interest (ROI) of an animal tissue sample for WAXS analysis was the focus.

Different methods have been used to assess the fibroglandular/fat content (breast density) *in vivo* since the knowledge provides a way to estimate the risks of developing cancer.[18–23] As Yaffe[24] summarizes, different qualitative and quantitative

methods have been applied to evaluate breast density. Examples of visual classification methods are the Wolfe density categories[18] and the Breast Imaging Reporting and Data System (BI-RADS).[25] More reliable computer-aided breast density measurements for quantitative analysis were developed.[26] The gray level thresholding method is a 2D technique where either a radiologist or a fully automated computer-assisted segmentation software chooses the threshold level to categorize the dense versus nondense regions. 3D x-ray breast imaging techniques may prove to be more useful since they overcome the limitations of overlapping structures. Dedicated breast CT (Refs. 27 and 28) and breast tomosynthesis[29] are two methods that are currently under development.

Although the task to estimate breast density in a breast biopsy is simpler, it is not trivial. Histology analysis of thin (e.g., 5 μm) sections of tissue can be used to estimate the composition of samples (e.g., Ref. 14). There is, however, no guarantee that the composition of the chosen slice(s) is the same throughout the sample. Geraki *et al.*[30] used XRF and EDXRD for the quantification of elemental concentrations in breast tissue. They found elevated concentrations of iron, copper, zinc, and potassium in malignant specimens.

Because the attenuation coefficients (μ) of fat are significantly different from those of cancer and fibroglandular tissue,[31] an x-ray imaging method was used to estimate $\overline{v}_{fat}$ in the volume of tissue (i.e., ROI) that was interrogated during the WAXS measurement. A ROI with animal fat and meat (fibrous, fib) tissue was used in this work. A WAXS fat subtraction model, validated in a previous work,[32] was used to estimate the differential linear scattering coefficient μ_s of the nonfat (fib) tissue. Refer to Ref. 32 for detailed descriptions of the WAXS system and validations of the WAXS models for acquisitions of μ_s. Section 2 briefly describes the WAXS component.

2. WAXS COMPONENT

Consider the interrogation of a 5 mm diameter $d = 4$ mm thick breast biopsy with a 2.7 mm diameter 50 kV beam. The ROI consists of a cylindrical volume defined by the intersection of the beam and sample. Let the mean fractional volumes of fat and fib tissue within the ROI be $\overline{v}_{fat}$ and $\overline{v}_{fib}$, respectively. The scatter coefficient of this mixture of tissue can be approximated by[32]

$$\overline{\mu}_s(x) = \frac{N_s(E,\theta)}{N_0(E)\Omega_{det}} \times \frac{\overline{\mu}(E)(1-\frac{1}{\cos\theta})e^{\overline{\mu}(E)\frac{d}{\cos\theta}}}{[1-e^{-\overline{\mu}(E)d(1-\frac{1}{\cos\theta})}]}, \quad (1)$$

where $N_s(E,\theta)$ is the scatter spectrum captured with a CdTe energy dispersive x-ray detector positioned at angle $\theta = 6°$ subtending $\Omega_{det} = 7.75 \times 10^{-5}$ sr, $N_0(E)$ is the incident spectrum, and $\overline{\mu} = \overline{v}_{fat}\mu_{fat} + \overline{v}_{fib}\mu_{fib}$. From this measurement, the μ_s of fib can be approximated by

$$\mu_{sc}(fib) = [\overline{\mu}_s - \overline{v}_{fat}\mu_s(fat)]/\overline{v}_{fib}, \quad (2)$$

where the subscript "c" denotes that the μ_s was obtained via subtraction (correction) of fat and μ_s(fat) is the scatter coefficient for a pure sample of fat. The $\overline{v}_{fat}$ within the ROI of

composite samples was estimated via the technique described in Sec. 3.B.

$\overline{\mu}_s$ for the mixture was compared to $\overline{\mu}_s^{\Sigma} = \overline{\nu}_{\text{fat}}\mu_s(\text{fat}) + \overline{\nu}_{\text{fib}}\mu_s(\text{fib})$, where $\mu_s(\text{fib})$ is the scatter coefficient for a pure fib sample. An agreement between $\mu_{sc}(\text{fib})$ and $\mu_s(\text{fib})$ would validate the fat subtraction protocol.

3. METHOD

3.A. Animal tissue

Chicken and beef tissue were acquired from a local butcher shop. Tissue was visually separated into two types: fat and fibrous tissue. These samples were labeled as pure samples. In addition, composite samples consisting of fibrous and fat components were prepared. The cylindrically shaped tissue samples of 5 mm diameter were fixed in formalin for 4 months. Following fixation, 4 mm thick samples were prepared.

3.B. Fat estimation technique

The fat estimation technique entails the generation of digital x-ray images of the tissue samples with an MX-20 digital specimen radiography system [Faxitron Bioptics (LLC), Tucson, AZ]. It consists of a stationary tungsten anode tube and a 2×2 in. phosphor screen coupled to a 1×1 in. CCD camera via a 2:1 fiber optic taper. The focal spot size is 25 μm and there are 1024×1024 24.8 μm detector pixels. The samples were imaged at a magnification 2 using 26 kV, 0.3 mA, and 3.8 s exposure times. The entrance exposure per image was 9.2×10^{-4} C/kg.

The MX-20 was calibrated with polyethylene (polyet) and polymethyl methacrylate (PMMA) samples each 5 mm in diameter and thicknesses ranging from 1 to 5 mm. The energy incident signal (EIS) upon a given pixel of area A_{pixel} was calculated using

$$\text{EIS} = \sum_j E_j \Phi_0(E_j) A_{\text{pixel}} e^{-(\mu_{\text{polyet}}(E_j)d_{\text{polyet}} + \mu_{\text{PMMA}}(E_j)d_{\text{PMMA}})},$$

(3)

where the incident photon fluence $\Phi_0(E)$ shown in Fig. 1(a) was estimated using a CdTe detector collimated with a 25 μm

diameter tungsten aperture. The μ values were calculated using cross section data for elements of Plechaty *et al.*[33] and the mixture rule.[34] The CCD detector pixel values are denoted by ADU to represent analog to digital units. Figure 1(b) shows the calibration curve fitted with a line of best fit given by

$$\text{ADU}_{\text{fit}}(\text{EIS}) = \text{m} \times \text{EIS} + \text{b},$$

(4)

where $\text{m} = (7.72 \pm 0.13) \times 10^{-3}$ ADU/keV and $\text{b} = (-31.3 \pm 34.1)$ ADU.

The $\overline{\nu}_{\text{fat}}$ within the 2.7 mm diameter 4 mm thick ROI was determined as follows. Consider the columns of tissue defined by the intersections of beamlets and pixels. Within the ROI there were 9533 columns. Each tissue column of thickness d was assumed to be composed of a mixture of fibrous and fat tissue. Let ν_{fat} denote the fractional volume of fat for a particular column. Calculations of

$$\text{EIS}(\nu_{\text{fat}}) = \sum_{j=1} E_j \Phi_0(E_j) A_{\text{pixel}} e^{-(\mu_{\text{fib}}(E_j)(1-\nu_{\text{fat}}) + \mu_{\text{fat}}(E_j)\nu_{\text{fat}})d},$$

(5)

as a function of ν_{fat} ranging from 0 to 1 were calculated using the attenuation coefficients μ of breast tissue.[31] Figure 1(c) shows plots of $\text{EIS}(\nu_{\text{fat}})$ versus ν_{fat} for samples of thickness $d = 1, 2, 3, 4,$ and 5 mm. The line corresponding to $d = 4$ mm was used in this work to estimate ν_{fat} for each column of tissue. Note that for whatever thickness of biopsy one can generate the required $\text{EIS}(\nu_{\text{fat}})$ versus ν_{fat} curve. The calculated $\text{EIS}(\nu_{\text{fat}})$ [Eq. (5)] that matched the EIS obtained via the ADU-EIS calibration [rearrangement of Eq. (4) with ADU_{fit} replaced with the ADU pixel value] yielded ν_{fat} for the column. The mean value $\overline{\nu}_{\text{fat}}$ was calculated for the ROI and its uncertainty was estimated as follows. EIS lower and upper bounds were calculated, namely

$$\text{EIS}^{\text{lower}} = \text{EIS} - \sigma_c,$$

(6)

$$\text{EIS}^{\text{upper}} = \text{EIS} + \sigma_c,$$

(7)

per pixel, where

$$\sigma_c^2 = \left(\frac{\partial \text{EIS}}{\partial \text{m}}\right)^2 \sigma_m^2 + \left(\frac{\partial \text{EIS}}{\partial \text{b}}\right)^2 \sigma_b^2$$

$$+ \left(\frac{\partial \text{EIS}}{\partial \text{ADU}}\right)^2 \sigma_{\text{ADU}}^2 - 2\text{mb}\,\text{Cov(m,b)}.$$

(8)

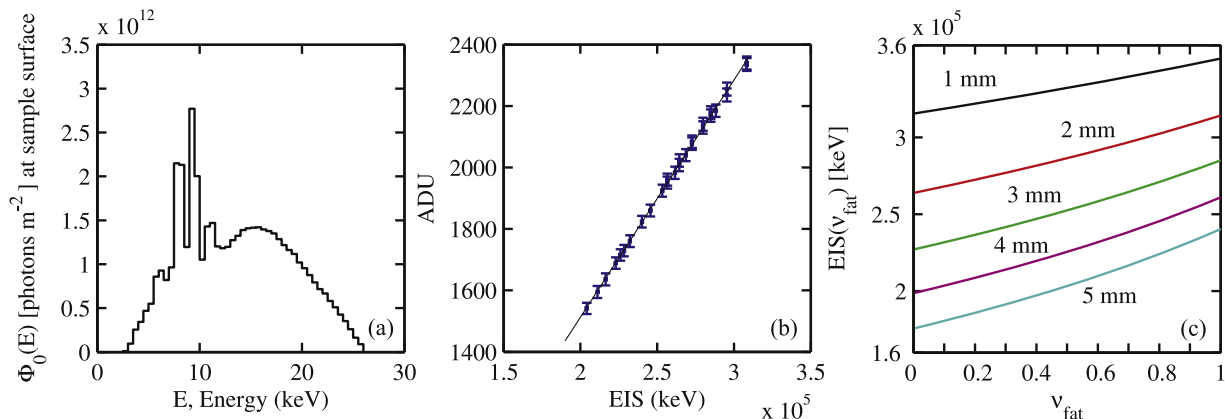FIG. 1. (a) Φ_0 estimated using a CdTe detector (measurement parameters: 26 kV, 30 s exposure, 25 μm diameter aperture, 8320 counts/s, 2.2 s dead time), and calibration curves (b) ADU versus EIS using PMMA and polyet plastics, and (c) EIS versus ν_{fat} for various thicknesses.

The error in ADU units ($\sigma_{ADU} = 19.9$) was taken to be the mean value of the standard deviations of ROI pixels values for all plastic samples. From the calibration curve [Fig. 1(c)], corresponding v_{fat} bounds were extracted per pixel. The means of the bounds were taken and their differences from $\bar{v}_{fat}$ provided an uncertainty range.

Simulations, as described next, were performed to determine whether $\bar{v}_{fat}$ is sufficient for the application of the fat subtraction model.

3.C. Simulations

Consider the 5 mm diameter 4 mm thick sample shown in Fig. 2(a) which was filled with fib and fat tissue voxels. The samples were divided into $0.1 \times 0.1 \times 0.1$ mm^3 voxels of which 22 400 (560×40) occupied the central ROI (regions 1 and 2). The ROI voxels were filled three different ways: (i) region 1 consisted of tissue columns with $v_{fib} = 0.6/v_{fat} = 0.4$, region 2 with 0.4fib/0.6fat, (ii) region 1: 0.4fib/0.6fat, region 2: 0.6fib/0.4fat, and (iii) tissue columns in the ROI were filled such that their v_{fat} distribution was a Gaussian ($\bar{v}_{fat} = 0.5$, $\sigma = 0.08$).

(a)

(b)

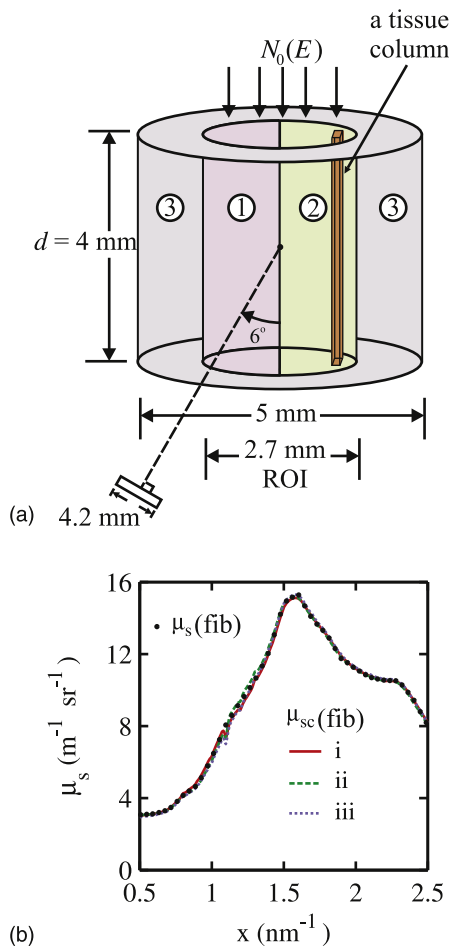FIG. 2. (a) Three sample configurations: (i) region 1 consisted of tissue columns with $v_{fib} = 0.6/v_{fat} = 0.4$, region 2 with 0.4fib/0.6fat, (ii) region 1: 0.4fib/0.6fat, region 2: 0.6fib/0.4fat, and (iii) tissue columns in the ROI were filled such that their v_{fat} distribution was a Gaussian ($\bar{v}_{fat} = 0.5$, $\sigma = 0.08$). (b) μ_{sc}(fib) signals via applications of the fat subtraction model.

The volume of the ROI consisted of 50% fib and 50% fat for all cases. The voxels within each column were filled randomly. For configurations i and ii, the column's v_{fat} distributions within the ROI were dual peaked, whereas Gaussian shaped for iii. As shown later in Sec. 4, they were Gaussian distributions for the tissue samples. The outer regions labeled as 3 were filled with fib yet filling them with fat gave similar results. This indicated that the outer region composition need not be included in the WAXS models.

The scattering was assumed to occur at the center of each voxel. Only single scatter was considered and statistical noise was not included in the simulations. The coherent form factors F used in the calculations were those measured by Poletti *et al.*[35] The incoherent scattering functions S were calculated using S of atoms from Hubbell *et al.*[36] and the sum rule.[37] The compositions used were those from Poletti *et al.*[35] The attenuation coefficients for fib and fat were taken from Johns and Yaffe.[31]

The μ_{sc}(fib) curves obtained via the subtraction model for the three sample configurations are shown in Fig. 2(b). The μ_s of fib which was sought is also shown. Although there are small differences between the curves, the subtraction works regardless of which type of v_{fat} distribution existed. The findings suggest that only $\bar{v}_{fat}$ is required for the application of the models and knowing the distributions of v_{fat} within the ROI of the sample is not necessary.

3.D. μ measurements

The analysis [i.e., Eqs. (1), (2), and (5)] was also done using μ values measured with the WAXS system in the $\theta = 0°$ configuration. However, a smaller 25 μm diameter aperture was used. A two basis function[31] method with aluminum and polycarbonate as bases was used to fit μ versus energy curves for fat and fibrous tissue. To obtain the curves, a 50 kV spectrum was used and the N_0 was estimated using a transmission measurement through a 4 mm thick PMMA sample. For an
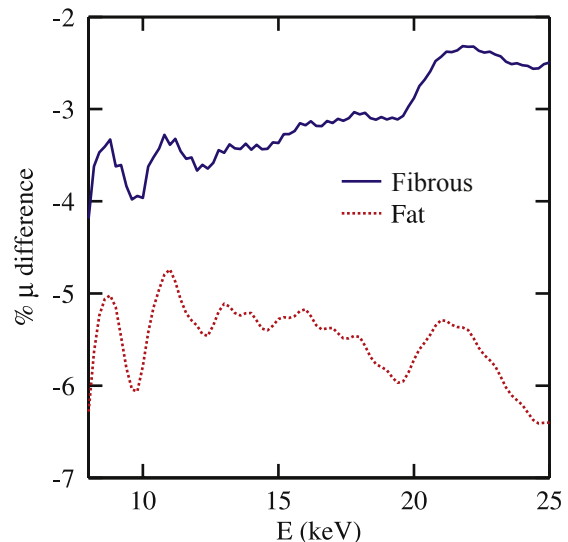

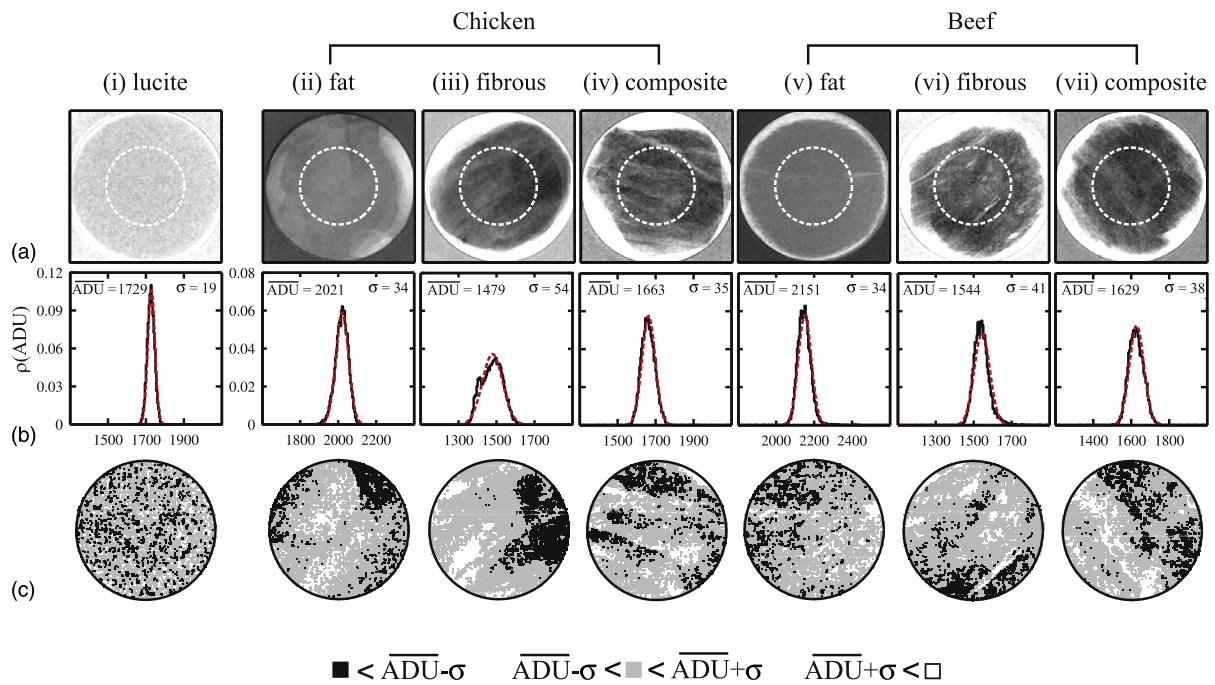FIG. 3. Comparisons of μ for chicken versus breast (Ref. 31) tissue.

FIG. 4. (a) Digital x-ray images, (b) ADU histograms, and (c) ADU maps.

energy range 8–25 keV, singular value decomposition was used to solve the system.

The results of μ measured (μ-expt) for chicken fat and fibrous were compared to those of breast tissue (μ-breast)[31] via the percent differences which are shown in Fig. 3. The results suggest that μ values of chicken tissue are similar to those of breast tissue. The differences (e.g., for chicken fat -5.8% smaller at 19 keV) could be caused by the fact that the samples were fixed in formalin, whereas those used by Johns and Yaffe[31] were unfixed tissue specimens. The duration
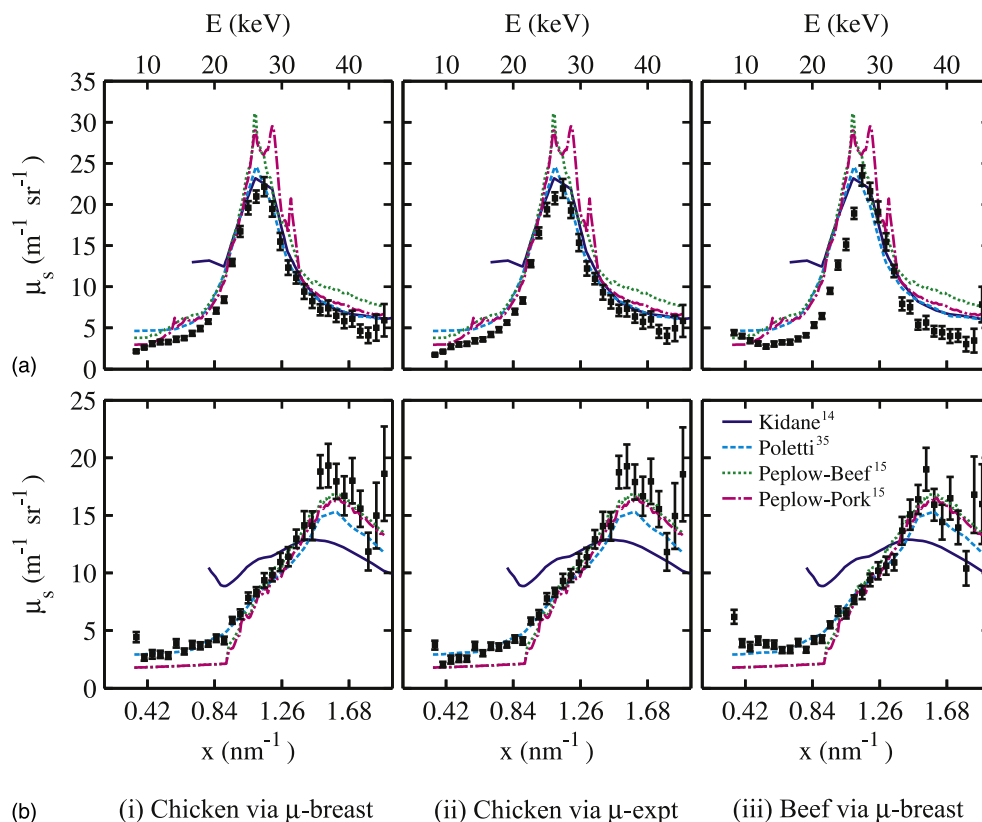

FIG. 5. μ_s of tissue (a) fat and (b) fibrous via (i) and (iii) μ-breast and (ii) μ-expt.

between sample extraction from formalin solution to actual transmission measurement could cause differences. Values of μ for beef were measured but deemed unacceptable because of this duration. The analysis of beef was only done with μ-breast values. Although optimization of μ measurements will be needed, the results in Sec. 4 were interesting and encouraging.

4. RESULTS AND DISCUSSIONS

Figure 4(a) shows images of (i) a PMMA sample, chicken samples of (ii) fat, (iii) fibrous, and (iv) fibrous that contains some fat (chicken composite), and beef (v) fat, (vi) fibrous, and (vii) composite samples. The dashed white lines in each image were added to highlight the ROI that corresponds to a 2.7 mm diameter central region. For the tissue samples, the corresponding ROI volume was interrogated during the WAXS measurements. The $\overline{\nu}_{fat}$ within the ROI volume was estimated for the composite samples.

The thickness of tissue at the outer edges varied a lot especially for the fibrous and the chicken composite samples. With better tissue preparation, the shape of the samples will look more like that of the plastic sample. However, it is the μ_s of the tissue within the ROI which was sought via WAXS measurements. The material outside the ROI, as mentioned in Sec. 3.C, was involved only in attenuating a small portion of the scattered photons from reaching the CdTe detector during the WAXS measurements. The beef fibrous image has some white streaks suspected to be caused by fat tissue.

Figure 4(b) shows corresponding histograms of the ADU values within the ROI. Their means and standard deviations are given in each figure and they were used to plot the Gaussian distributions (dashed lines). These Gaussians approximate the distributions except for the chicken fibrous sample [Fig. 4(b)(iii)]. This sample's ROI thickness deviated from uniformity. In a future work, a new tissue cutting apparatus will provide consistent accurate uniform thicknesses for the samples.

Figure 4(c) shows ADU maps. Pixels are displayed as gray unless they have an ADU beyond 1 σ of the mean, in which case as black (<) or white (>). The maps are meant to highlight any possible features within the ROI that would appear as clustered regions. The map for PMMA [Fig. 4(c)(i)] displays a mottle pattern while those of the tissue have mottle characteristics yet some clustering is seen. The map for beef fibrous [Fig. 4(c)(vi)] has clusters caused by fat streaks while the larger clusters occurring for chicken fibrous [Fig. 4(c)(iii)] were caused by a nonuniform thickness. Although deviations from purity and thickness uniformity occurred, the WAXS results shown below for all samples were encouraging.

Figure 5 shows the μ_s values for tissue (a) fat and (b) fibrous samples. (i) and (ii) are for chicken tissue using, respectively, μ-breast and μ-expt while panel (iii) is for beef using μ-breast. Also shown are μ_s for breast tissue from Kidane *et al.*;[14] μ_s for breast tissue calculated using F data from Poletti *et al.*,[35] S from Hubbell *et al.*[36] with compositions from Poletti *et al.*;[35] and μ_s for animal tissue calculated using F data from Peplow and Verghese,[15] S from Hubbell *et al.*[36] with compositions

from ICRU Report 46.[38] The 1.1 nm^{-1} fat peak signal is seen in the fat samples. These fibrous data are similar to each other except for the Kidane *et al.*[14] fibroglandular breast tissue. The μ_s of chicken obtained using μ-breast were similar to those obtained with μ-expt.

Figure 6 shows the ν_{fat} distributions for the chicken and beef composites. The ROIs' ν_{fat} distributions were well approximated by Gaussians (dashed lines) obtained using the $\overline{\nu}_{fat}$ and σs (see figure) of each distribution. The FWHMs are indicated via the arrows. For the chicken composite, $\overline{\nu}_{fat} = 0.4 \pm 0.05$ via use of μ-breast, 0.33 ± 0.05 using μ-expt, and 0.32 ± 0.05 for the beef composite using μ-breast.

Figure 7 shows that $\overline{\mu}_s$ values for the composites match well with $\overline{\mu}_s^\Sigma$. The root mean square deviations Δ_{rms} between them are also shown. The results for chicken were slightly better when μ-expt were used. Figure 8 shows that $\mu_{sc}(fib)$ obtained via the fat subtraction model matched closely the $\mu_s(fib)$ obtained with a pure fibrous sample. Again for chicken, better results (i.e., smaller Δ_{rms}) were obtained using μ-expt. Although the results for beef with μ-expt were poor (not shown), the results obtained using μ-breast were satisfactory. The differences $\overline{\mu}_s - \overline{\mu}_s^\Sigma$ and $\mu_{sc}(fib) - \mu_s(fib)$ were computed and their mean values were compared to 0 via t-tests. The null hypothesis was retained for all samples verifying that the mean of differences
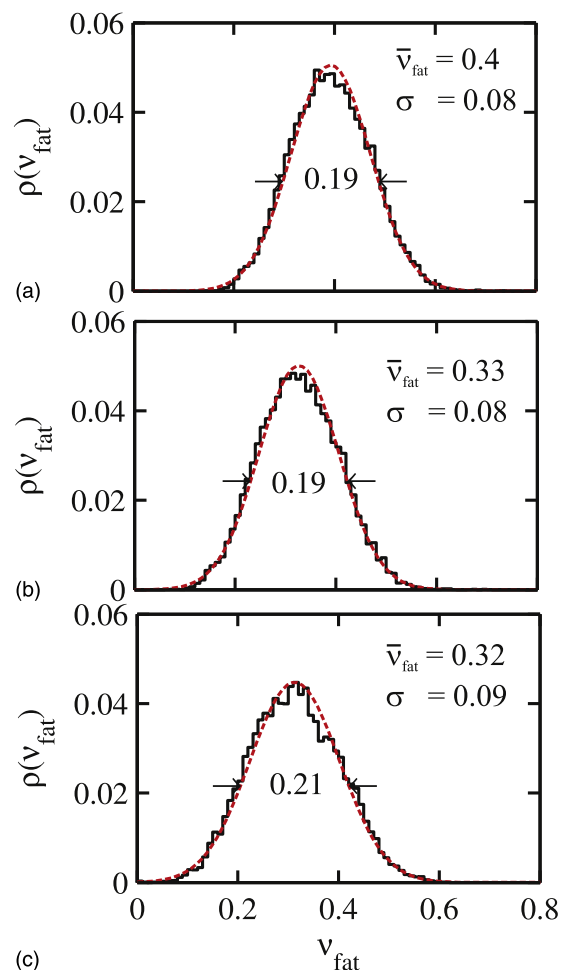

FIG. 6. ν_{fat} distributions of the chicken composite via (a) μ-breast and (b) μ-expt, and of the (c) beef composite via μ-breast.
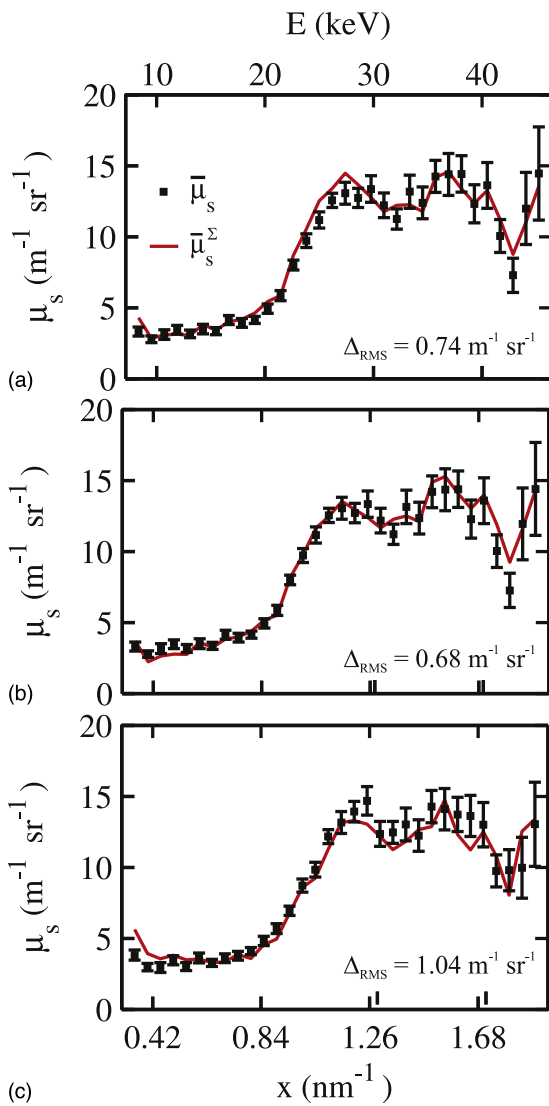
FIG. 7. $\overline{\mu}_s$ of the chicken composite via (a) μ-breast and (b) μ-expt, and of (c) the beef composite via μ-breast.
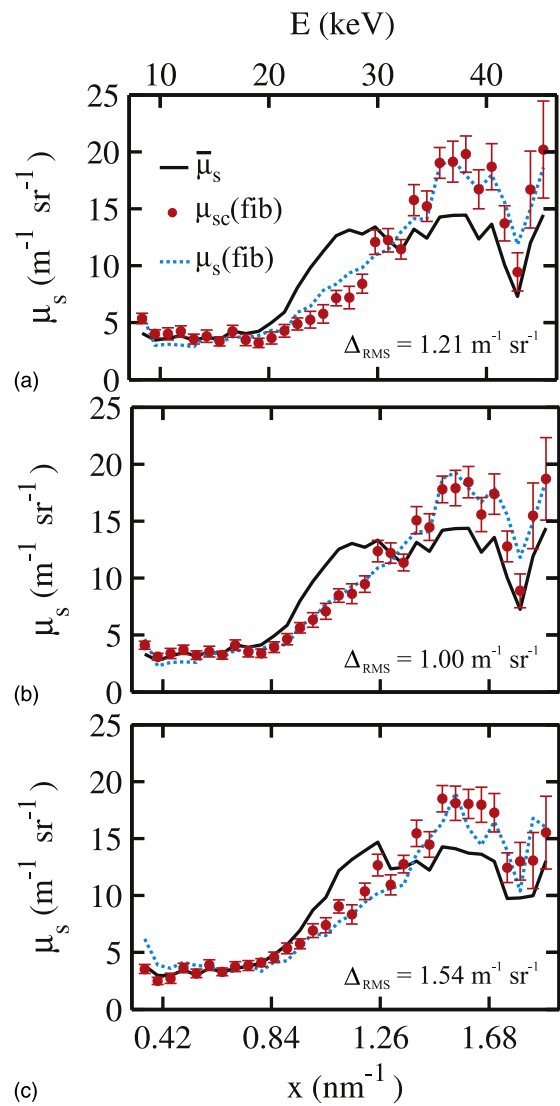

FIG. 8. μ_{sc} of fibrous tissue via the fat subtraction model applied to the chicken composite using (a) μ-breast, (b) μ-expt, and to (c) the beef composite using μ-breast.

did not vary from the expected mean of 0 in a statistically significant way. The Δ_{rms} and t-test were two ways of comparing the distributions, yet a more quantitative measure will be developed. The findings validate the use of the technique for estimating $\overline{\nu}_{fat}$ for the applications of the WAXS models.

5. FUTURE WORK

The next phase to the research program is to refine the fat estimation and subtraction protocol. The selection of only two tissue types fat and fibrous was sufficient to demonstrate the usefulness of the methods, however, the reproducibility of our measurements need to be verified. The measurements of μ and the sample preparation (especially its thickness) will be optimized since they need to be known accurately for Eq. (5). The elapsed time between tissue extraction from formalin and μ measurement needs to be maintained consistent for all samples. The purity of our baseline pure samples will be quantified via combined μ and image analysis. Namely, μ values determined for a 25 μm diameter column of the tissue sample will be

measured. The sample will then be imaged and its fat content will be estimated using the measured μ. For a pure sample of fat, ν_{fat} should be equal to 1, whereas $\nu_{fat} = 0$ for a pure fibrous sample. Measurements at 2° and 12° with a higher 80 kV beam will allow a larger region of momentum transfer to be probed. Uncertainties will be reduced with a higher kV beam and with a beam stopper to reduce air scatter ($\approx 15\%$). The effects caused by the CdTe detector response will need to be assessed for the higher kV analysis.[39]

Since the scatter signals from the amorphous samples are circularly symmetric, a detector matrix of CZT pixels[40] would allow a larger portion of the scattered field to be captured thereby reducing the uncertainty. However, at this time, such a detector is not available to the research program.

6. CONCLUSIONS

The methodology to estimate $\overline{\nu}_{fat}$ within a ROI of a tissue sample for use in a WAXS fat subtraction model was shown

to be quantitatively accurate. Optimizations of this procedure are under way and the analysis of breast biopsies will commence shortly.

ACKNOWLEDGMENTS

[a]Electronic mail: rx_tang@laurentian.ca

[b]Electronic mail: mcdnancye@gmail.com

[c]Electronic mail: cx_laamanen@laurentian.ca

[d]Author to whom correspondence should be addressed. Electronic mail: rleclair@laurentian.ca

[1]M. J. Farquharson, A. Al-Ebraheem, S. Cornacchi, G. Gohla, and P. Lovrics, "The use of x-ray interaction data to differentiate malignant from normal breast tissue at surgical margins and biopsy analysis," X-Ray Spectrom. **42**, 349–358 (2013).

[2]A. L. C. Conceição, M. Antoniassi, and M. E. Poletti, "Preliminary study of human breast tissue using synchrotron radiation combining WAXS and SAXS techniques," Appl. Radiat. Isot. **68**, 799–803 (2010).

[3]W. M. Elshemey, O. S. Desouky, M. M. Fekry, S. M. Talaat, and A. A. Elsayed, "The diagnostic capability of x-ray scattering parameters for the characterization of breast cancer," Med. Phys. **37**, 4257–4265 (2010).

[4]S. Pani, E. J. Cook, J. A. Horrocks, J. L. Jones, and R. D. Speller, "Characterization of breast tissue using energy-dispersive X-ray diffraction computed tomography," Appl. Radiat. Isot. **68**, 1980–1987 (2010).

[5]V. Changizi, A. A. Kheradmand, and M. A. Oghabian, "Application of small-angle X-ray scattering for differentiation among breast tumors," J. Med. Phys. **33**, 19–23 (2008).

[6]O. R. Oliveira, A. L. C. Conceição, D. M. Cunha, M. E. Poletti, and C. A. Pelá, "Identification of neoplasias of breast tissues using a powder diffractometer," J. Radiat. Res. **49**, 527–532 (2008).

[7]J. A. Griffiths, G. J. Royle, A. M. Hanby, J. A. Horrocks, S. E. Bohndiek, and R. D. Speller, "Correlation of energy dispersive diffraction signatures and microCT of small breast tissue samples with pathological analysis," Phys. Med. Biol. **52**, 6151–6164 (2007).

[8]E. A. Ryan and M. J. Farquharson, "Breast tissue classification using x-ray scattering measurements and multivariate data analysis," Phys. Med. Biol. **52**, 6679–6696 (2007).

[9]D. M. Cunha, O. R. Oliveira, C. A. Pérez, and M. E. Poletti, "X-ray scattering profiles of some normal and malignant human breast tissues," X-Ray Spectrom. **35**, 370–374 (2006).

[10]R. J. LeClair, M. M. Boileau, and Y. Wang, "A semianalytic model to extract differential linear scattering coefficients of breast tissue from energy dispersive x-ray diffraction measurements," Med. Phys. **33**, 959–967 (2006).

[11]E. A. Ryan and M. J. Farquharson, "Angular dispersive x-ray scattering from breast tissue using synchrotron radiation," Radiat. Phys. Chem. **71**, 971–972 (2004).

[12]C. R. F. Castro, R. C. Barroso, M. J. Anjos, R. T. Lopes, and D. Braz, "Coherent scattering characteristics of normal and pathological breast human tissues," Radiat. Phys. Chem. **71**, 649–651 (2004).

[13]M. E. Poletti, O. D. Gonçalves, and I. Mazzaro, "Coherent and incoherent scattering of 17.44 and 6.93 keV x-ray photons scattered from biological and biological-equivalent samples: characterization of tissues," X-Ray Spectrom. **31**, 57–61 (2002).

[14]G. Kidane, R. D. Speller, G. J. Royle, and A. M. Hanby, "X-ray scatter signatures for normal and neoplastic breast tissues," Phys. Med. Biol. **44**, 1791–1802 (1999).

[15]D. E. Peplow and K. Verghese, "Measured molecular coherent scattering form factors of animal tissues, plastics and human breast tissue," Phys. Med. Biol. **43**, 2431–2452 (1998).

[16]L. R. M. Morin, "Molecular form factors and photon coherent scattering cross sections of water," J. Phys. Chem. Ref. Data **11**, 1091–1098 (1982).

[17]B. Alberts, A. Johnson, J. Lewis, M. Raff, K. Roberts, and P. Walter, *Molecular Biology of the Cell*, 5th ed. (Garland Science, New York, NY, 2008).

[18]J. N. Wolfe, "Breast patterns as an index of risk for developing breast cancer," Am. J. Roentgenol. **126**, 1130–1137 (1976).

[19]J. N. Wolfe, "Risk for breast cancer development determined by mammographic parenchymal pattern," Cancer **37**, 2486–2492 (1976).

[20]V. A. McCormack and I. d. S. Silva, "Breast density and parenchymal patterns as markers of breast cancer risk: A meta-analysis," Cancer Epidemiol., Biomarkers Prev. **15**, 1159–1169 (2006).

[21]N. F. Boyd, H. Guo, L. J. Martin, L. Sun, J. Stone, E. Fishell, R. A. Jong, G. Hislop, A. Chiarelli, S. Minkin, and M. J. Yaffe, "Mammographic density and the risk and detection of breast cancer," N. Engl. J. Med. **356**, 227–236 (2007).

[22]C. M. Vachon, V. S. Pankratz, C. G. Scott, S. D. Maloney, K. Ghosh, K. R. Brandt, T. Milanese, M. J. Carston, and T. A. Sellers, "Longitudinal trends in mammographic percent density and breast cancer risk," Cancer Epidemiol., Biomarkers Prev. **16**, 921–928 (2007).

[23]M. J. Yaffe, N. F. Boyd, J. W. Byng, R. A. Jong, E. Fishell, G. A. Lockwood, L. E. Little, and D. K. Tritchler, "Breast cancer risk and measured mammographic density," Cancer Epidemiol., Biomarkers Prev. **7**, 47–55 (1998).

[24]M. Yaffe, "Mammographic density. Measurement of mammographic density," Breast Cancer Res. Treat. **10**(3), 209–218 (2008).

[25]American College of Radiology, *Breast Imaging Reporting and Data System (BIRADS)* (American College of Radiology, Reston, VA, 1993).

[26]J. A. Harvey and V. E. Bovbjerg, "Quantitative assessment of mammographic breast density: Relationship with breast cancer risk," Radiology **230**, 29–41 (2004).

[27]J. M. Boone, T. R. Nelson, K. K. Lindfors, and J. A. Seibert, "Dedicated breast CT: Radiation dose and image quality evaluation," Radiology **221**, 657–667 (2001).

[28]A. O'Connell, D. L. Conover, Y. Zhang, P. Seifert, W. L. Young, C. L. Lin, L. Sahler, and R. Ning, "Cone-beam CT for breast imaging: Radiation dose, breast coverage, and image quality," Am. J. Roentgenol. **195**, 496–509 (2010).

[29]C. M. Shafer, E. Samei, and J. Y. Lo, "The quantitative potential for breast tomosynthesis imaging," Med. Phys. **37**, 1004–1016 (2010).

[30]K. Geraki, M. J. Farquharson, and D. A. Bradley, "X-ray fluorescence and energy dispersive x-ray diffraction for the quantification of elemental concentrations in breast tissue," Phys. Med. Biol. **49**, 99–110 (2004).

[31]P. C. Johns and M. J. Yaffe, "X-ray characterization of normal and neoplastic breast tissues," Phys. Med. Biol. **32**, 675–695 (1987).

[32]R. Y. Tang, C. Laamanen, N. McDonald, and R. J. LeClair, "WAXS fat subtraction model to estimate differential linear scattering coefficients of fatless breast tissue: Phantom materials evaluation," Med. Phys. **41**, 053501 (7pp.) (2014).

[33]E. F. Plechaty, D. E. Cullen, and R. J. Howerton, "Tables and graphs of photon interaction cross sections from 1.0 keV to 100 MeV derived from the LLL evaluated nuclear data library," UCRL-50400, Vol. 6, Revision 1, Lawrence Livermore Laboratory, 1975.

[34]F. H. Attix, *Introduction to Radiological Physics and Radiation Dosimetry* (John Wiley & Sons, New York, 1986).

[35]M. E. Poletti, O. D. Gonçalves, and I. Mazzaro, "X-ray scattering from human breast tissues and breast-equivalent materials," Phys. Med. Biol. **47**, 47–63 (2002).

[36]J. H. Hubbell, Wm. J. Veigele, E. A. Briggs, R. T. Brown, D. T. Cromer, and R. J. Howerton, "Atomic form factors, incoherent scattering functions, and photon scattering cross sections," J. Phys. Chem. Ref. Data **4**, 471–538 (1975); **6**, 615–616(E) (1977) (Erratum).

[37]R. J. LeClair and P. C. Johns, "A semianalytic model to investigate the potential applications of x-ray scatter imaging," Med. Phys. **25**, 1008–1020 (1998).

[38]ICRU, "Photon, electron, proton, and neutron interaction data for body tissues," ICRU Report 46 (ICRU, Bethesda, MD, 1992).

[39]R. J. LeClair, Y. Wang, P. Zhao, M. Boileau, L. Wang, and F. Fleurot, "An analytic model for the response of a CZT detector in diagnostic energy dispersive x-ray spectroscopy," Med. Phys. **33**, 1329–1337 (2006).

[40]J. S. Iwanczyk, E. Nygard, O. Meirav, J. Arenson, W. C. Barber, N. E. Hartsough, N. Jalakhov, and J. C. Wessel, "Photon counting energy dispersive detector arrays for x-ray imaging," IEEE Trans. Nucl. Sci. **56**, 535–542 (2009).